Construction and Building Materials 220 (2019) 386–395

Contents lists available at ScienceDirect

Construction and Building Materials

journal homepage: www.elsevier.com/locate/conbuildmat

Effects of the variety and content of coal gangue coarse aggregate on the mechanical properties of concrete

Mei Zhou [a], Yanwei Dou [a,*], Yuzhuo Zhang [b], Yuanqiang Zhang [a], Boqun Zhang [a]

[a] College of Civil Engineering, Liaoning Technical University, Fuxin 123000, China
[b] College of Civil Engineering, Shenyang Jianzhu University, Shenyang 110168, China

HIGHLIGHTS

- The macro and micro characteristics of coal gangue and natural gravel are analyzed.
- The failure modes of concrete with different coal gangue aggregates are revealed.
- The relationship between microstructure and macrobehavior of concrete is described.
- The stress-strain curve model of concrete with different aggregates is established.

ARTICLE INFO

Article history:
Received 31 December 2018
Received in revised form 25 May 2019
Accepted 28 May 2019
Available online 11 June 2019

Keywords:
Coal gangue
Spontaneous combustion gangue
Rock gangue
Strength characteristics
Stress-strain curve
Microstructure

ABSTRACT

Concrete were prepared by replacing natural gravel (N) with spontaneous combustion gangue (S) or rock gangue (R) at intervals of 25%. Mechanical tests were carried out and the microstructural features of the concrete were characterized. Failure modes and strength of different concrete are various, and the compressive strength of the concrete meets the design requirements of C30 strength grade concrete. The axial compression failure mode of R coarse aggregate concrete (RAC) was shear failure. As the S replacement percentage increased, the axial compression failure mode of S coarse aggregate concrete (SAC) transformed from shear failure to longitudinal splitting failure. The ITZ of SAC is the best; as the replacement percentage increased, the peak stress and slope of the rising section of the stress-strain curves of RAC and SAC decreased, and the peak strains increased. Finally, compressive stress-strain curve prediction models for coal gangue coarse aggregate concrete were suggested.

© 2019 Elsevier Ltd. All rights reserved.

1. Introduction

China is a large country with coal as its main energy source. The annual output of coal gangue solid waste, which is produced during coal production, amounts to hundreds of millions of tons. A large amount of coal gangue is stored for a long time, and such storage can destroy the ecological balance and harm the environment. Statistics show that among the more than 2100 counties in China, extensive coal gangue accumulation has been reported in more than 1200 counties. Currently, the amount of accumulated coal gangue is approximately 4.5 billion tons, and there are more than 1600 coal gangue mounds that occupy approximately 15,000 ha of land; moreover, the quantity of gangue accumulation is increasing at a rate of 1.5–200 million tons per year [1,2]. With the rapid development of infrastructure construction in China, raw materials such as sand and stone, which are used in concrete, the most common engineering materials, must be urgently supplied. In the summer of 2018, the prices of sand and stone in the Pearl River Delta (China) area exceeded 300 RMB/ m^3, resulting in a price increase of 700 RMB/m^3 for C30 ready-mixed concrete, which has caused panic in the industry [3,4]. Coal gangue is also called a 'resource in the wrong place'. Although there are many varieties of coal gangue, which are relatively nonhomogeneous and have varying properties, the chemical and mineral compositions of a large portion of the accumulated gangue are similar to those of natural aggregate. Under feasible technological and reasonable economic conditions, from a scientific perspective, determining how to promote the coal gangue industry in the market and enhance the use of coal gangue aggregate are important subjects worthy of extensive study. Because the formation mechanism of coal gangue varies in each region of China, there are large differences in the physical, chemical and mineral compositions of the gangue. Additionally, there are different technical requirements for coal gangue aggregates in coal gangue aggregate concrete used

* Corresponding author.
E-mail address: YW_D0102@126.com (Y. Dou).

https://doi.org/10.1016/j.conbuildmat.2019.05.176
0950-0618/© 2019 Elsevier Ltd. All rights reserved.

in different engineering applications. Therefore, scientific analyses of the basic properties of coal gangue (such as water absorption, firmness, crushing value, etc.) are necessary to ensure that coal gangue aggregate concrete meets all structural safety requirements at normal temperatures and can be used normally under high- and low-temperature conditions. Considering the output and accumulation of industrial waste around the world, scholars from Europe and Japan have studied concrete prepared from recycled concrete, marble and granite cutting waste [5–8]. In addition, Chinese scholars have conducted many studies of coal gangue aggregate concrete and tailings slag aggregate concrete. Notably, Chen [9], Zhou et al. [10], Zhang et al. [11], and Wang et al. [12] studied the preparation and basic properties of coal gangue aggregate concrete and found that it is feasible to prepare concrete using coal gangue as the coarse aggregate. Duan [13] established the inner connection between the microstructure and macromechanical performance of coal gangue aggregate concrete. Dong et al. [14] studied the effects of different active aggregate mortar strengths through microscopic tests. Wang et al. [15] found that it is possible to produce grade-30 coal gangue concrete with coarse and fine coal gangue aggregates. In addition, Li et al. [16] showed that preparing concrete with coal gangue aggregate is practical and that the concrete drying shrinkage performance and freezing resistance performance meet the Chinese engineering specifications. However, most of these studies focused on SAC, few studies have focused on rock gangue aggregate concrete. Additionally, research on the constitutive properties of coal gangue aggregate concrete is rare. A better understanding of the basic properties of coal gangue coarse aggregate concrete could lead to new theoretical findings, new methods and new technologies for engineering applications involving coal gangue coarse aggregate concrete. In this research, according to the rock characteristics of coal gangue, representative samples of spontaneous combustion (S) and rock (R) sandstone gangue, which are similar to natural gravel, are selected to prepare coarse aggregates. By means of step-by-step substitution, mechanical tests of concrete compression, split tension, bending resistance, axial compression and stress-strain were performed on 120 specimens of different sizes. Additionally, the microstructure characteristics and the constitutive relations with the macroscopic behaviors of the concrete are described using SEM and XRD techniques. A corresponding theoretical model is established to provide a reference for the calculations and analyses of the structure of coal gangue aggregate concrete.

2. Experimental program

2.1. Preparation and main technical properties of coarse aggregate

Two varieties of coal gangue coarse aggregates with different properties (S and R) were used. Both S and R samples were supplied from Qinghemen Mine of the Fuxin Mining Group, Northeast China. After being crushed with a jaw crusher, sieved, classified and blended, coal gangue coarse aggregates (S and R) with 5 ~ 20 mm of continuous gradation were obtained. Natural gravel (N) was obtained from local quarries. The macroscopic and microscopic morphologies of the three different coarse aggregates are given in Figs. 1 and 2, respectively. The main pore size distribution is shown in Fig. 3. The main mineral composition is shown in Fig. 4, and the details of the main chemical compositions are listed in Table 1. The main technical properties of the three coarse aggregates were tested according to the standard for technical requirements and test method of sand and crushed stone (or gravel) for natural aggregate concrete (JGJ52-2006) [17], and the results are shown in Table 2. The quality of the coal gangue coarse aggregates

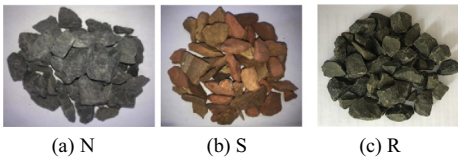

(a) N (b) S (c) R

Fig. 1. Appearance of the coarse aggregates.

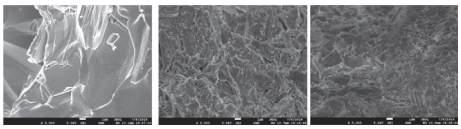

(a) N (b) S (c) R

Fig. 2. SEM photos of the coarse aggregates.

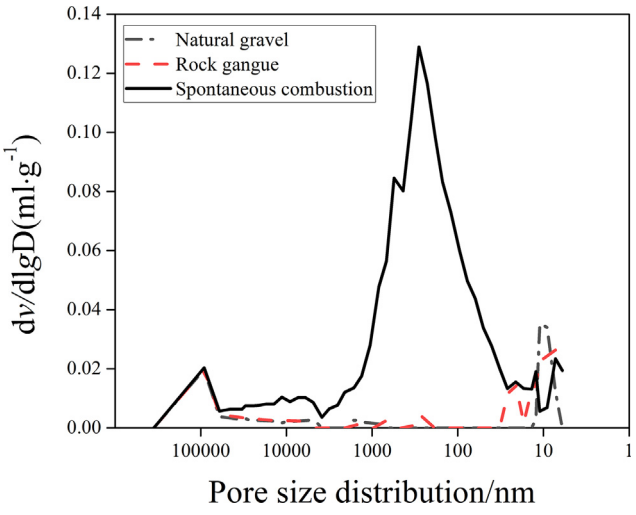

Fig. 3. Pore size distribution of three different coarse aggregates.

was evaluated based on the standard for recycled coarse aggregate for concrete (GB/T5177-2010) [18].

2.1.1. Macroscopic and microscopic morphology of coarse aggregates

Figs. 1 and 2 clearly show that the macroscopic and microscopic morphologies of the three different coarse aggregates are quite different. Notably, there are dark red, pottery red, pottery yellow and light soils in S. The degree of spontaneous combustion of S in nature varies, and S is highly heterogeneous with a high content of needle-shaped flakes. The hardness of the S samples is lower than that of the N and R samples, and the structure is loose and porous. R is black or black gray, and the homogeneity level and needle-shaped flake content are between those of S and N. There are black and gray attachments on the surface. Additionally, the hardness of R is higher and the structure is denser with fewer pores than S, but it is not as dense as N. N is light gray, and the corresponding homogeneity, grain shape and gradation are superior compared to the properties of S and R. Additionally, the N samples displayed the highest density.

2.1.2. Chemical constituents and mineral compositions

As shown in Table 1 and Fig. 4, the main chemical constituents of the two types of coal gangue are SiO_2 and Al_2O_3, and the main mineral components are quartz and gismondine. The contents of these oxides were even higher than those for local natural gravel.

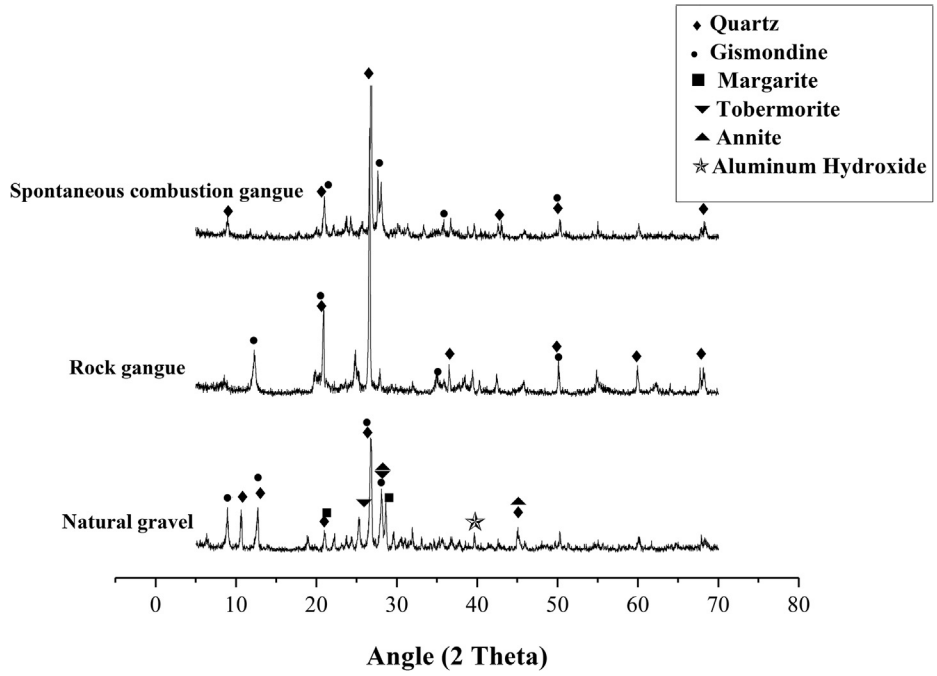

Fig. 4. XRD spectra of the coarse aggregates.

Table 1
Main chemical constituents of the three different coarse aggregates.

Aggregates	SiO_2	Al_2O_3	Fe_2O_3	CaO	MgO	TiO_2	Na_2O	K_2O	SO_3	P_2O_5	Cl	MnO
N	46.84	15.79	15.75	8.34	6.90	0.89	1.80	2.72	0.24	0.33	0.10	0.06
S	55.57	21.00	6.57	3.65	2.50	0.84	1.90	4.10	0.82	0.24	0.1	2.50
R	50.28	26.31	6.11	7.74	2.00	1.13	1.10	3.28	0.93	0.15	0.16	0.07

Table 2
Basic properties of the three different coarse aggregates.

Aggregates	Properties						
	Apparent density/kg·m^{-3}	Bulk density /kg·m^{-3}		Void ratio/%	Water absorption/%	Sturdiness/%	Crushed value/%
		Loose density	Tap density				
N	2705	1470	1660	45.66	0.83	1.3	4.5
S	2276	1075	1220	52.77	7.55	8.3	21.2
R	2653	1340	1489	49.49	3.15	1.5	9.9

By comparing the chemical constituents and mineral components of coal gangue with the classification standard of rock [19,20], it can be preliminarily determined that both R and S are types of sandstone gangue and that their properties are similar to those of N, so they are suitable for use as aggregates in concrete.

2.1.3. Apparent density and void ratio

The apparent density (ρ_0) and void ratio (P_o') of the coarse aggregate indicate that N meets the requirements of Class I coarse aggregate ($\rho_0 > 2450$ kg/m^3, $P_o' < 47\%$), R meets the requirements of Class II coarse aggregate ($\rho_0 > 2350$ kg/m^3, $P_o' < 50\%$), and S meets the requirements of Class III coarse aggregate ($\rho_0 > 2250$ kg/m^3, $P_o' < 53\%$).

2.1.4. Water absorption and crushing value

The water absorption (W_m) values of the coarse aggregate indicate that N meets the Class I requirement ($W_m < 3\%$), R meets the Class II requirement ($W_m < 5\%$), and S meets Class III requirements ($W_m < 8\%$). Additionally, the crushing values (Q_a) indicate that N and R meet the Class I requirement ($Q_a < 12\%$) and that S meets the Class III requirement ($Q_a < 30\%$).

As dispersed particles in concrete, coarse aggregate has a large influence on the apparent density, elastic modulus and volume deformation of concrete. The particle size, grain shape, water absorption ability and crushing value of coarse aggregate have a greater influence on the mechanical properties of concrete than do that of the chemical constituents and mineral composition [21]. The two types of coal gangue coarse aggregates used in this study have different grain shapes, densities and crushing values because of the differences in the formation process, production process or porosity. Although there are considerable differences between the properties of S and R, and they are obviously different from those of N. According to the standard of "Recycled coarse aggregate for concrete" (GB/T5177-2010) [18], these materials still meet the requirements for different grades of coarse aggregate for concrete.

2.2. Other raw materials

The cementitious materials used in this study are Fuying 42.5R ordinary Portland cement, grade I fly ash and grade S95 mineral powder. The fine aggregate is local river sand with a fineness

modulus of 3.16. In addition, the coarse aggregate, except S and R, is local 5–20 mm continuous gradation natural gravel (N). The mixing water was normal tap water. Polycarboxylate superplasticizer was used to maintain the slump of fresh concrete at a constant level, the dosage of which was 1.5–2.5%, and the water reduction rate was 20–30%.

2.3. Experimental design

The preparation requirements of concrete in this research were as follows. The slump values of fresh concrete should be greater than 160 mm. In addition, the strength of hardened concrete should meet the strength requirements of C30. Using a stepwise replacement method, the percentages of R and S considered were 25%, 50%, 75% and 100%, respectively. Additionally, natural aggregate concrete (NAC) with N served as the control group. Therefore, a total of nine groups of concrete with designed mix proportions were studied, as listed in Table 3. Because S has a large porosity and high water absorption, prewetting was performed 1 h ahead of time, and the additional water was that at 60% of the 1-hour water absorption rate; this process was implemented to ensure that the concrete mixture meets the relevant construction requirements [22].

For each mix proportion, cubic specimens with dimensions of 100 mm × 100 mm × 100 mm and prismatic specimens of 100 mm × 100 mm × 300 mm and 100 mm × 100 mm × 400 mm were prepared. Three specimens were prepared for each set of dimensions. In addition, three 100 mm × 100 mm × 300 mm prismatic specimens with 50% and 100% replacement percentages of SAC and RAC were prepared and used to assess the accuracy of the stress-strain fitting equations. Therefore, a total of 120 concrete specimens were prepared. All specimens were demolded after 24 h of casting and then cured under standard curing conditions (T = 20 ± 2°C, RH ≥ 95%) for 28 days.

2.4. Experimental loading method

After being cured for 28 days, according to the Standard for Test methods of Mechanical Properties of natural aggregate concrete (GB/T50081-2002) [23], the Standard Test Method for Compressive Strength of Cylindrical Concrete Specimens (ASTM C 39/C 39 M-2018) [24] and the Standard Practice for Making and Curing Concrete Test Specimens in the Laboratory (ASTM C 192/C 192 M-2018) [25], the mechanical properties of concrete were tested. The compressive and splitting tensile strength were determined on 100 mm cubic specimens; the axial compressive strength, elastic modulus and the stress-strain curves were measured on 100 mm × 100 mm × 300 mm prismatic specimens; and the flexural strength was tested with 100 mm × 100 mm × 400 mm prismatic specimens. The compressive and axial compressive strengths were measured by a 100 T electrohydraulic servo universal testing machine, and the loading system for the axial compression test was controlled by displacement with a loading rate of 0.01 mm/s. The test device and the loading diagram are shown in Fig. 5. In the stress-strain test, the stress-strain curves of the concrete specimens were recorded with a DH3817k data acquisition system, and the period of data acquisition was 0.02 s. The splitting tensile strength and flexural strength were measured by a 30 T electrohydraulic servo universal testing machine, and the loading device used in the flexure test is shown in Fig. 6.

Fig. 5. Test device and loading diagram for the concrete stress-strain curve test. Note: 1. Steel ring frame 2. Displacement meter 3. Specimen 4. Pressure sensors.

Real-time micro-scanning electron microscopy was performed on the abovementioned groups of specimens. After the cubic compressive strength test, the interface between the cement matrix and aggregate was selected from the fragments. The observation surface of the specimens was required to be as smooth as possible, as small and light as possible, and not more than 1 cm^3. The specimens were pumped into a vacuum for scanning electron microscopy analysis. The microstructure of the samples was observed using a Japanese electronic JSM- 7500F cold field emission scanning electron microscope.

3. Results and analysis

3.1. Failure characteristics

The different varieties of coal gangue coarse aggregate concrete with different replacement percentages exhibited failure processes

Table 3
Mixed proportions of concrete with different types of coarse aggregate ($kg \cdot m^{-3}$).

Types		Materials							
		Cement	Fly ash	Mineral powder	Water	Water reducing agent	Fine aggregate	Coarse aggregates	
								N	S or R
NAC		324	93	46	210	1.5	628	1025	0
RAC/%	25	328	94	47	190	8.64	626	766	255
	50	328	94	47	190	8.64	626	511	511
	75	328	94	47	190	8.64	626	255	766
	100	328	94	47	190	8.64	626	0	1025
SAC/%	25	324	97	43	223	1.38	632	774	268
	50	324	97	43	237	1.38	632	536	536
	75	324	97	43	253	1.38	632	268	774
	100	324	97	43	268	1.38	632	0	1031

Notes: 1) NAC – represents natural aggregate concrete. RAC − 25, RAC − 50, RAC − 75 and RAC − 100 represent RAC with replacement percentages of 25%, 50%, 75%, and 100%, respectively. SAC − 25, SAC − 50, SAC − 75 and SAC − 100 represent SAC with replacement percentages of 25%, 50%, 75%, and 100%, respectively.
2) The water in (SAC) consists of mixing water and additional water, and the additional water is 60% of the 1-hour water absorption rate.

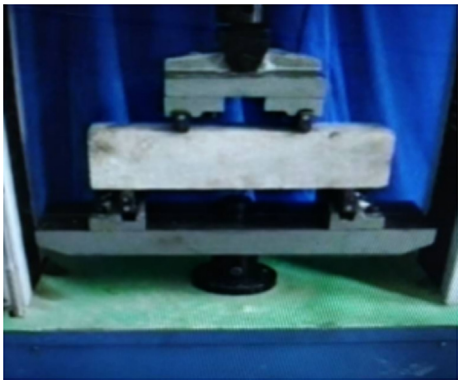

Fig. 6. Loading device for the four-point flexure test of concrete.

and failure modes similar to those of natural aggregate concrete under a uniaxial force, but each displayed distinct characteristics, and the results are shown in Figs. 7–9.

Fig. 7 shows that the failure modes of RAC and NAC are similar, and two 'quadrilateral cones', which are inversely connected, formed after the failure of concrete under compression. Cracks mainly occurred at the interface between R and the cement matrix and inside the cement matrix. The failure sections of SAC are different from those of SAC and NAC. For SAC, because of the low strength of S itself, the development of the cracks was almost unhindered by the coarse aggregates, and the fracture sections directly penetrated the material in the final failure of concrete, so they were relatively smooth. For RAC, although the mechanical properties of R and the cement mortar matrix are better than those of N, which should have led to fewer interface cracks in the concrete, the interfacial bonding between R and the cement matrix is greatly affected by the powder material attached to the R surface. As a result, as the replacement percentage of R increases, the negative effect becomes more significant, and the probability of interfacial bond failure in the RAC increases. Moreover, the stresses at interface cracks in SAC were obviously higher than those in RAC because S is influenced by internal curing and surface activation effects. Additionally, the strength of S was close to the strength of the cement matrix. However, the critical stress ratio was not affected by the strength. Therefore, for SAC, the stress change was small when the cracks developed from the interface cracks to the bond cracks and eventually matrix cracks. In addition, S did not act as a crack brake. When the concrete was under compression, the fracture surface expansion of SAC was almost unhindered by S, and cracks directly penetrated the coarse aggregates.

As Fig. 8(a) shows, as the S replacement percentage increases, the axial compression failure mode of SAC gradually changes from shear failure to vertical split failure, and a 'cone' obviously forms after failure. The main reason for this result is that the compression failure of SAC begins with the tensile cracking of mortar, and then these cracks penetrate S. The S at the failure surface is almost completely broken, and the fracture section is smooth. The enhanced interface area around S in SAC and its better elastic coordination with the cement mortar lead to few interface cracks. When the load increases to 90%-95% of the ultimate load, visible cracks parallel to the load direction appear on the surface of the specimen. Because of the low strength of S itself and the expansion of the fracture surface, which is not hindered by S, as the S

(a) RAC-100 (b) SAC-100

Fig. 7. Compressive failure modes of different varieties of coal gangue coarse aggregate concrete.

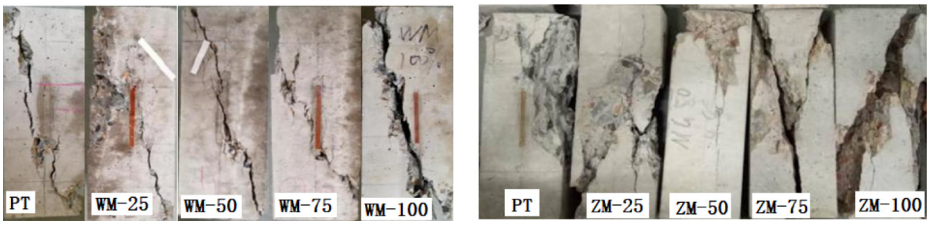

(a) Shear failure of RAC (b) splitting failure of SAC

Fig. 8. Axial compression failure modes of different varieties of coal gangue coarse aggregate concrete with different replacement percentages.

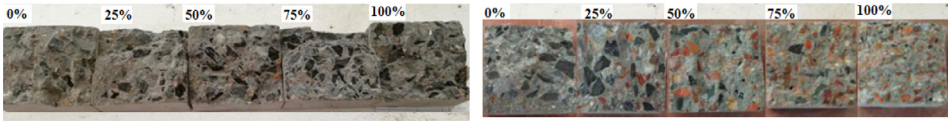

(a) RAC (b) SAC

Fig. 9. Splitting failure sections of different varieties of coal gangue coarse aggregate concrete with different replacement percentages.

replacement percentage increases, the SAC failure surface develops continuous cracks running through the whole specimen, resulting in comminuted failure. As Fig. 8(b) shows, shear failure occurs in all RAC specimens. As the R replacement percentage increases, the width of the surface cracks increases gradually during the axial compression failure of RAC, and the missing angle of the specimens becomes increasingly obvious. In this case, the specimen exhibits typical brittle failure characteristics. The failure mode of RAC under axial compression is similar to that of NAC. In the failure mode of RAC under axial compression, cracks go around the coarse aggregate and develop along the main interface crack. At the beginning of loading, the RAC prism specimen has no cracks on the concrete surface. When the load approaches the failure load, small vertical cracks begin to appear in the middle of the surface of the specimen, and there are a intermittent and subtle noises emitted from the interior of the specimen. When the failure load is reached, the vertical cracks rapidly develop into oblique cracks, and the concrete experiences oblique shear failure along the oblique cracks and loses its bearing capacity.

Fig. 9 shows that in the splitting tensile failure mode of SAC, all the large coarse aggregate particles penetrate the specimen, and almost no damage is found for the bond between S and the matrix. In the splitting tensile failure of RAC, most R is broken in the fracture section, and little damage occurs to the bonds between R and the cement matrix. Because there are more inherent defects in S and R than in N, as the replacement percentage increases, the splitting tensile strength of SAC and RAC considerably decreases in a discretized manner. Additionally, but also the splitting surface of SAC and RAC is smooth compared with that of NAC, which indicates that most of the coarse aggregates are cracked and destroyed.

3.2. Strength, axial compression ratio, tensile to compressive ratio and ratio of flexural to compressive strength

The cubic compressive strength (f_{cu}), splitting tensile strength (f_{ts}), axial compressive strength (f_{cp}) and flexural strength (f_{tm}) of different varieties of coal gangue coarse aggregate concrete with different replacement percentages were tested, and each result was the average of measurements for three specimens, as shown in Fig. 10(a)–(d). Fig. 10(a) shows that each group of concrete meets the design strength requirements for C30 concrete. A comparison of the strengths in Fig. 10(a)–(d) indicates that the f_{cu} and f_{cp} values of RAC are higher than those of SAC and that the f_{ts} and f_{tm} values are lower than those of SAC. For RAC, f_{cp}/f_{cu} varies from 0.67 to 0.77, and for SAC, this ratio ranges from 0.71 to 0.81. Moreover, f_{ts}/f_{cu} for RAC ranges from 1/14 to 1/19 and for SAC ranges from 1/13 to 1/17. Additionally, f_{tm} / f_{cu} for RAC varies from 1/11 to 1/14, and that for SAC ranges from 1/13 to 1/17. The results indicate that the ductility of SAC is better than that of RAC.

As the replacement percentage increases, the f_{cu} and f_{cp} values of SAC and RAC decrease, and the corresponding trends are the same. When the replacement percentage is less than 50%, the decrease in f_{cu} is large, but when the replacement percentage is greater than 50%, the decrease in f_{cu} becomes small, and the decrease in f_{cp} is not obvious. As the replacement percentage increases further, the f_{ts} values of SAC and RAC decrease initially and then increase, and f_{ts} reaches a minimum when the replacement percentage is 50%. The variations in the f_{ts} values of SAC and RAC with increasing replacement percentage are different. Notably, the f_{ts} value of RAC decreases with increasing replacement percentage, and the f_{ts} value of SAC increases initially and then decreases with increasing replacement percentage. When the replacement percentage is the same, the f_{ts} value of SAC is obviously larger than that of RAC.

In addition, the f_{ts} values of SAC and RAC are discrete, and even when the replacement percentage is 50%, the f_{ts} values cannot meet the design requirements. Measures such as adding fibers or rubber particles could be implemented to increase f_{ts}.

3.3. The peak stress, peak strain and elastic modulus

Test data, such as the peak stress (σ_c), peak strain (ε_c) and elastic modulus (E_c) values for each group of concrete specimens, were obtained by performing uniaxial compression tests, and the results are listed in Table 4. Table 4 shows that with increasing S and R replacement percentages, the peak stress and elastic modulus of the concrete decrease, and the peak strain increases. The main reasons for these findings are as follows. (1) Because the apparent density of S and R is smaller than that of N, the apparent density and elastic modulus of concrete prepared by S and R decrease with increasing coal gangue replacement percentage. This finding is consistent with those of Feng Naiqian, who found 'the elastic modulus of concrete is proportional to the apparent density' [21]. (2) The homogeneity of R and S is worse than that of N. In particular, the proportion of low-quality aggregate in S is larger resulting in aggregates with a low elastic modulus, which in turn influences the elastic modulus of the concrete [21,26–27]. (3) Because S was loose, the S samples had high porosities. Porosity determines the stiffness of the aggregate, and stiffness controls the ability of the

Table 4
The peak stress, peak strain and elastic modulus test results for the concrete in each group.

Types of concrete		Peak stress /MPa	Peak strain /με	Elastic modulus /GPa
NAC		35.62	1582.34	31.40
RAC /%	25	33.48	1710.45	27.75
	50	32.13	1900.69	24.00
	75	31.26	1944.56	19.73
	100	30.57	2145.11	18.40
SAC /%	25	34.15	1878.26	27.50
	50	32.36	1865.90	26.92
	75	30.74	2176.73	22.87
	100	23.62	1970.76	13.46

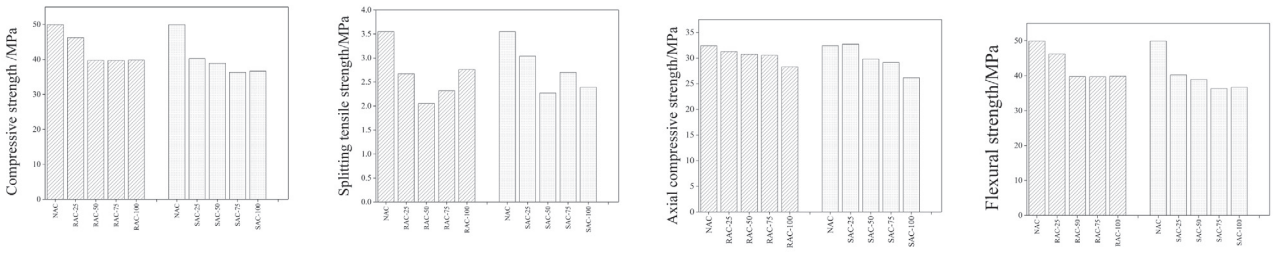

(a) Compressive strength (b) Splitting tensile strength (c) Axial compressive strength (d) Flexural strength

Fig. 10. Strength of different varieties of coal gangue coarse aggregate concrete with different replacement percentages.

aggregate to mitigate the strain of the cement matrix [28]. (4) Although the internal structure of R was relatively dense, the bonding strength between R and the cement matrix was ultimately affected by the powder materials attached to the surface of the R samples, resulting in decreases in σ_c and E_c.

3.4. Analysis of the characteristics and micromorphology of the interface transition zones

SEM photos were used to characterize the microstructures of typical concrete fragments in each group, as shown in Fig. 11. There were no obvious differences in the hydration products and hydration degrees of the concrete specimens in each group, but the microstructures of the interface transition zones (ITZs) and the coarse aggregates of each group were significantly different. Fig. 11(a)–(d) show that as the S replacement percentage increased, the ITZ of the concrete became thinner and denser, as shown in Fig. 11(e). This result can be attributed to two factors. First, S is characterized by loose porosity, and it absorbed the water from the surrounding cement matrix, which lowered the water-cement ratio in the ITZ. More importantly, S has an active surface that can react with the hydration products of cement, and the new hydration products entered the pores on the surface of the coarse aggregates, resulting in the coarse aggregates being firmly grasped by the cement matrix, which strengthened the ITZ. Therefore, there was no obvious boundary at the ITZ. Fig. 11(f)–(i) show that with the increase in the replacement percentage of R, the ITZ between the coarse aggregate and cement matrix gradually became thicker and looser, and the number of loose and porous particles with irregular shapes increased. Therefore, the ITZ was the weakest part of the RAC samples, mainly due to the negative influence of the powder materials attached to the surface of the coarse aggregates on the bonding strength between the aggregates and cement matrix. The microstructure characteristics of SAC and RAC were consistent with the macroscopic failure behaviors under uniaxial compression.

4. Establishment of a uniaxial compression-based full stress-strain curve model of coal gangue coarse aggregate concrete

4.1. Influence of the variety and content of coal gangue on the compressive stress-strain curves of concrete

The full stress-strain curves of the concrete under uniaxial compression varied with the varieties and replacement percentages of coal gangue coarse aggregates, as shown in Fig. 12. The variations in the rising sections of the stress-strain curves of the two different types of coal gangue coarse aggregate concrete are similar. As the replacement percentage increases, the slope of the rising sections and the peak stress decrease, and the peak strain increases, which suggests that the elastic modulus of the concrete decreases. However, the variations in the descending sections of the stress-strain curves were different. As the replacement percentage increased, the descending sections of the curves of RAC became steeper, the residual strength rapidly decreased, and the areas under the curves gradually decreased, indicating that the ductility of the concrete worsened. For SAC, the descending sections were flatter, the rate of decrease in the strength was slower, and the ultimate

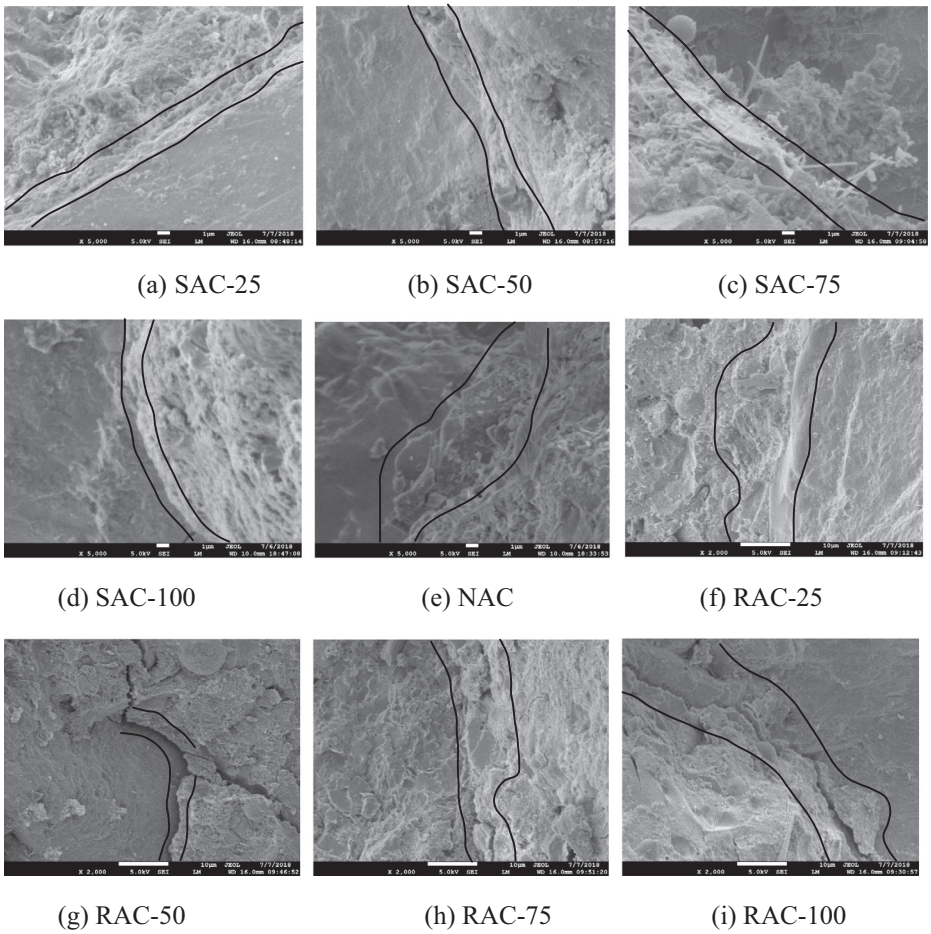

Fig. 11. SEM photos of concrete with different coal gangue types and different replacement percentages.

compressive strain gradually increased. These findings indicate that the ductility of SAC was better than that of NAC and RAC. This difference can be attributed to the structures of the aggregates being damaged during the mechanical preparation of samples, causing more microcracks to form inside the aggregates. Fig. 3 shows that S is porous. Compared with R and N, S with porous properties has larger deformation under stress and lower compressive and splitting strength, so the descending section slowly falls back, resulting in larger peak strain and smaller elastic modulus of SAC.

Fig. 12 shows that the peak stress of SAC is lower than that of RAC and the peak strain is similar in the two types of coarse aggregate concrete at the same replacement rate; however, the ultimate strain displays a large discrepancy. The ultimate strain of SAC is larger than that of RAC, and both are larger than that of NAC. Notably, the peak strain can reflect the deformation capacity of the concrete under loads, and the shapes of the descending sections of the stress-strain curves reflect the deformation capacities and energy absorption characteristics of the concrete. However, there was a large difference between the descending sections of the stress-strain curves for the concrete with the two types of coal gangue coarse aggregates. The deformation capacities and energy absorption characteristics of SAC were obviously better than those of RAC and NAC.

4.2. Establishing a stress-strain curve model for coal gangue coarse aggregate concrete

The uniaxial compressive stress-strain curves for different varieties of coal gangue concrete with different replacement percentages were converted into dimensionless standard curves ($x = \varepsilon/\varepsilon_c$, $y = \sigma/\sigma_c$). The results show that the geometry is similar to the stress-strain curve of natural aggregate concrete. Based on the model of Guo [29], as shown in Eq. (1), the stress-strain curve equation of coal gangue coarse aggregate concrete under compression is regressed, as shown in Table 4 and Fig. 13.

$$y = \begin{cases} ax + (3-2a)x^2 + (a-2)x^3, 0 \leqslant x \leqslant 1 \\ \frac{x}{b(x-1)^2+x}, x > 1 \end{cases} \quad (1)$$

where a reflects the variations in the deformation modulus of the concrete and b represents the size of the area encompassed by the descending sections and the strain axis.

By fitting the experimental data using the Marquardt method, the fitting parameters a and b of the concrete were obtained, as shown in Table 5. Only one parameter (a or b) is used in the ascending and descending sections of Guo's model, and a and b are independent; therefore, the two curves are fitted separately.

Table 5
Fitting parameters of the uniaxial compressive constitutive equations of the concrete.

Types of concrete	Parameters	Replacement percentages (%)				
		0	25	50	75	100
RAC	a	1.72	1.69	1.33	1.02	0.65
	b	2.26	2.58	7.87	10.22	11.89
SAC	a	1.72	1.36	1.31	1.24	1.20
	b	2.26	2.13	1.91	1.59	1.05

The changes in the a and b values reflect some important properties of concrete [29]. The rising section of stress-strain curve not only reflects the elastoplasticity of concrete specimens before failure but also the ability of the concrete to absorb and store energy to some extent. In SAC and RAC, with increases in the replacement percentages of S and R, the value of a decreases, indicating that the elastic modulus of concrete decreases. This change is mainly due to the high porosity of S and R, more micro-cracks compared with N and a low elastic modulus of coarse aggregate itself, which results a decrease in the elastic modulus of the concrete prepared as the replacement percentage increases.

For RAC, as the R replacement percentage increases, a decreases and b increases. Thus, the stress-strain curve becomes steeper, and the area under the curve becomes smaller. As the value of b increases, the descending section of the curve becomes steeper and the plastic deformation of the concrete decreases; additionally, the ductility is poor, the residual strength is low, the failure process is rapid, the toughness of the material decreases and the brittleness increases. For SAC, as the S replacement percentage increases, the values of a and b decrease. Compared with N and R, S exhibit larger deformation under stress and lower compressive and splitting tensile strengths, so the descending section of the curve slowly falls back, resulting in a small elastic modulus, large peak strain and high ultimate strain for SAC. This finding indicates that the ductility and energy absorption capacity of SAC are better than those of RAC and NAC. The results are in agreement with the findings in references 13 and 29.

The relationships between the parameters (a and b) and coal gangue replacement percentage (r) were established by regression analyses. For RAC and SAC, a and b can be calculated by Eqs. (2) and (3) respectively. The range of r is $0 < r \leq 100\%$, and the correlation coefficients (R^2) of the fitting parameters a and b were greater than 0.93.

$$\begin{cases} a = -0.0112\,r + 1.8440 \\ b = 0.1052\,r + 1.8240 \end{cases} \quad (2)$$

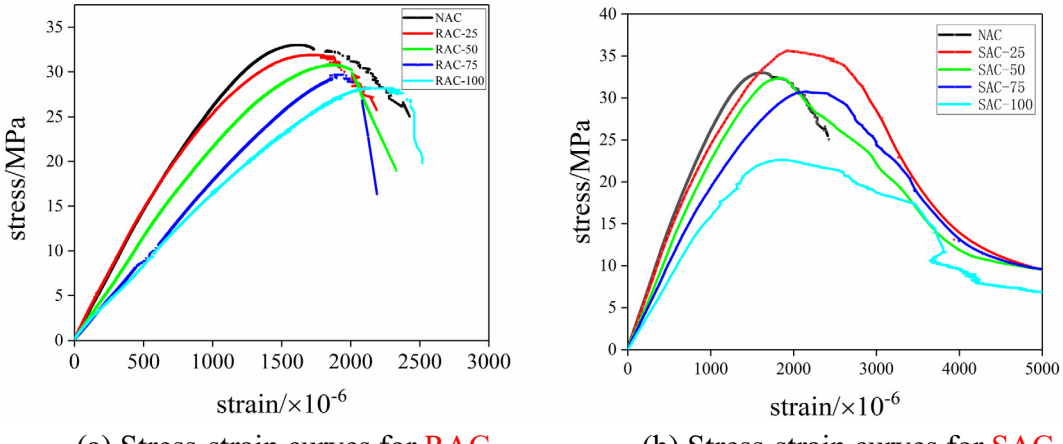

(a) Stress-strain curves for RAC (b) Stress-strain curves for SAC

Fig. 12. stress-strain curves for different types of coal gangue coarse aggregate concrete.

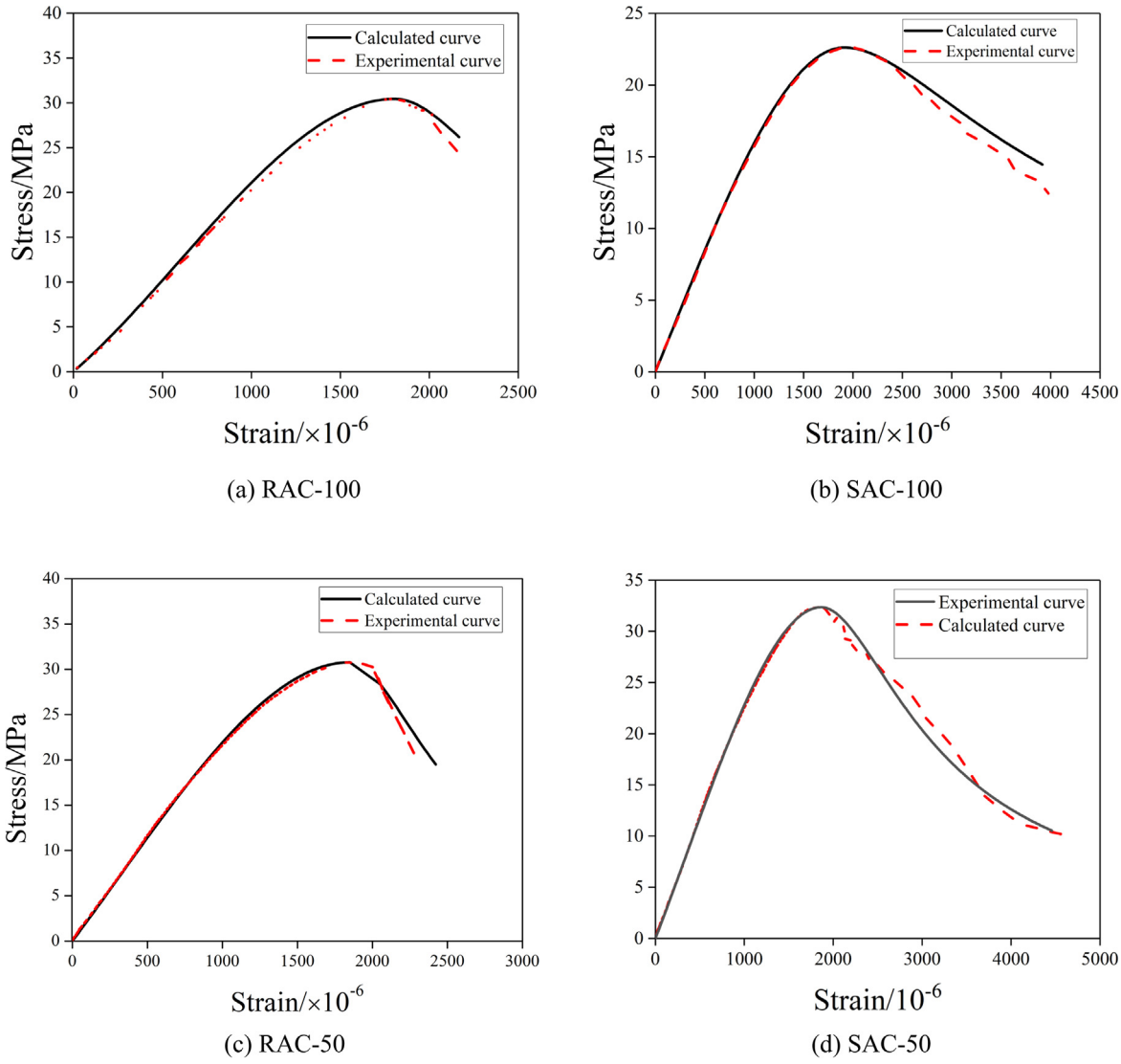

Fig. 13. Comparison of experimental and calculated stress-strain curves.

$$\begin{cases} a = 7 \times 10r^{-5} - 0.0117r^2 + 1.6866 \\ b = -0.0118r + 2.3800 \end{cases} \quad (3)$$

To test the accuracy of the fitting parameters, four representative groups of concrete (RAC-100, SAC-100, RAC-50 and SAC-50) were prepared, including three specimens in each group. A stress-strain curve test was conducted after standard curing for 28 days. Additionally, the parameters of a and b were calculated from Eqs. (2) and (3) and substituted into Eq. (1) to compare the experimental stress-strain curves and the calculated curves, as shown in Fig. 13. The rising sections of the compressive stress-strain curves established based on Guo's model were in good agreement with those of the calculated curves. In addition, the initial stage of the descending sections was consistent, but there were some differences in the later stage. However, for structural concrete, when the load value exceeds the failure load, internal cracks will penetrate the concrete, and the corresponding structure can no longer bear loads. However, the bearing capacity of the structure will not be affected. Therefore, the failure characteristics of the coal gangue coarse aggregate concrete can be most accurately explained by the descending sections of the stress-strain curve equations established in this research. In addition, Guo's model is still applicable for coal gangue coarse aggregate concrete, but there are some differences in the values of the parameters.

5. Conclusion

(1) S and R have different shapes, densities, porosity ratios, water absorption and crushing values due to their different origins and physical, chemical and mineral properties and preparation process. However, according to the characteristics of sandstone gangue and recycled coarse aggregate standard for concrete, it is feasible to replace N with S and R to prepare C30 pumping concrete.

(2) The failure processes and failure modes of RAC and SAC with different replacement percentages are similar, but each displays some distinct characteristics. The failure of RAC is mainly due to the interfacial bonding failure between R and the cement matrix. For SAC, most S in the fracture section is broken. The failure mode of RAC under axial compression involves the shear failure of oblique section. The failure mode of SAC under axial compression transforms from shear failure to longitudinal splitting failure as the replacement percentage increases.

(3) As the replacement percentage increases, the f_{cu} and f_{cp} values of RAC and SAC decrease, and f_{ts} first decreases and then increases. The f_{tm} value of RAC decreases as the replacement percentage increases, and the f_{tm} of SAC initially increases and then decreases. The splitting tensile strength of coal

gangue coarse aggregate concrete is relatively discrete and should be given more attention in the future. Measures such as adding fibers or rubber particles could be implemented to increase f_{ts}.

(4) As the replacement percentage increases, the slopes of the rising sections of the stress-strain curves and the peak stresses decrease, the peak strains increase, the crack width of RAC becomes wider, and the slopes of the descending section become steeper. Moreover, the slopes of the descending sections of the SAC stress-strain curves became more gradual, and the deformation capacity increases.

(5) The porosity, surface roughness and activity of S yielded a high-quality ITZ structure in the concrete, but it was still insufficient for overcoming the long-term strength shortage caused by S itself being broken. The bonding strength between R and the cement matrix was greatly affected by the powder materials attached to the surface of the R samples, and the ITZ was the weakest part of the RAC samples. Therefore, S and R were suitable for mixing medium and low-strength concrete.

(6) According to Guo's model, the constitutive relation model of coal gangue coarse aggregate concrete under compression was preliminarily established and displayed high accuracy, providing a new theory for structure analyses of coal gangue coarse aggregate concrete and a new method for engineering applications.

Conflict of Interest

None.

Acknowledgements

The financial support by the Coal Joint Fund of the National Natural Science Foundation of China (No. U1261122) and the Youth Science Fund of the National Natural Science Foundation (No. 51808352) is gratefully acknowledged.

References

[1] H.J. Li, Comprehensive Utilization of Coal Gangue, Chemical Industry Press, Beijing, 2010.
[2] H. Li, Prediction of the present situation and development trend of the sand aggregate industry in China, The Memoirs of the Second China Sand Aggregate Industry Investment Development (Hangzhou) Summit, China, 2017.
[3] J.L. Chen, Y.X. Fang, Present situation and problems of concrete aggregates in China, Architect. Technol. 36 (1) (2005) 23–25.
[4] Industry Information, The sand in the Pearl River Delta area is out of stock, and concrete enterprise is forced to stop supplying, Jiangxi Build. Mater. 9 (2018) 86.
[5] X.Y. Cong, S. Lu, Y. Yao, Z. Wang, Fabrication and characterization of self-ignition coal gangue autoclaved aerated concrete, Mater. Des. 97 (2016) 155–162.
[6] B.S. Thomasa, A. Damareb, R.C. Guptac, Strength and durability characteristics of copper tailing concrete, Constr. Build. Mater. 48 (2013) 894–900.
[7] S. Singh, S. Khan, R. Khandelwal, A. Chugh, R. Nagar, Performance of sustainable concrete containing granite cutting waste, J. Clean. Prod. 119 (15) (2016) 86–98.
[8] S. Singh, R. Nagar, V. Agrawal, Performance of granite cutting waste concrete under adverse exposure conditions, J. Clean. Prod. 127 (20) (2016) 172–182.
[9] B.P. Chen, Feasibility of applying coal gangue to the aggregate, J. Huaqiao U. (Nat. Sci.) 15 (2) (1994) 181–184.
[10] M. Zhou, G.N. Li, Q. Zhang, H.B. Cui, Study on application of spontaneous combustion coal gangue aggregate in ready-mixed concrete, J. Build. Mater. 18 (05) (2015) 830–835.
[11] J.X. Zhang, W.L. Chen, R.J. Yang, Experimental study on basic properties of coal gangue aggregate, J. Build. Mater. 13 (6) (2010) 739–743.
[12] C.L. Wang, W. Ni, S.Q. Zhang, S. Wang, G.S. Gai, W.K. Wang, Preparation and properties of autoclaved aerated concrete using coal gangue and iron ore tailings, Constr. Build. Mater. 104 (2016) 109–115.
[13] X.M. Duan, J.W. Xia, J.P. Yang, Influence of coal gangue fine aggregate on microstructure of cement mortar and its action mechanism, J. Build. Mater. 17 (4) (2014) 700–705.
[14] Z.C. Dong, J.W. Xia, C. Fan, J.C. Cao, Activity of calcined coal gangue fine aggregate and its effect on the mechanical behavior of cement mortar, Constr. Build. Mater. 100 (2015) 63–69.
[15] Z.S. Wang, N. Zhao, Influence of coal gangue aggregate grading on strength properties of concrete, Wuhan U. J. Nat. Sci. 20 (1) (2015) 66–72.
[16] Y.J. Li, Y. Xing, X. Zhang, X.P. Yan, Experimental study on the durability of the concrete with coal gangue aggregate, J. China Coal Soc. 38 (7) (2013) 1215–1219.
[17] People's Republic of China Industry Standard, Standard for technical requirements and test method of sand and crushed stone (or gravel) for ordinary concrete (JGJ52-2006), Ministry of Construction of the People's Republic of China, Beijing, 2006.
[18] People's Republic of China National Standard, Recycled coarse aggregate for concrete (GB/T5177-2010), Standards Press of China, Beijing, 2010.
[19] Z.S. Xu, Q.W. Yang, X.G. Wang, Z.N. Wang, Classification and comprehensive utilization of coal gangue, Chin. Environ. Prot. Ind. 7 (2001) 24–27.
[20] D.M. Wang, Y.F. Zuo, Q. Li, D.K. Fan, Y.S. Cui, W.L. Wang, Mineralogy characteristics of coal gangue and resource utilization of building materials, Brick & Tile. 6 (2006) 17–23.
[21] N.Q. Feng, High Performance Concrete Structure, Mechanical Industry Press, Beijing, 2004.
[22] M. Zhou, B.C. Pu, M. Xu, B.Y. Tian, Q. Zhong, Effect of additional water and prewet time on the performance of spontaneous combustion gangue sand lightweight concrete, B. Chin. Ceram. Soc. 32 (12) (2013) 2421–2426.
[23] People's Republic of China National Standard. Standard for test method of mechanical properties on ordinary concrete (GB/T 50081-2002), Ministry of Construction of the People's Republic of China, Beijing, 2002.
[24] ASTM C39/C39M-18, Standard Test Method for Compressive Strength of Cylindrical Concrete Specimens, West 2018 Conshohocken, PA.
[25] ASTM C192/C192M-18, Standard Practice for Making and Curing Concrete Test Specimens in the Laboratory, West 2018 Conshohocken, PA.
[26] A.M. Neville, Properties of Concrete, Longman, London, 1995.
[27] J.Z. Xiao, J.T. Du, Full stress-strain curves of different recycled coarse aggregate concrete under uniaxial compression, J. Build. Mater. 11 (2) (2008) 111–115.
[28] F. Salguero, J.A. Grande, T. Valente, R. Garrido, M.L. de la Torre, J.C. Fortes, A. Sánchez, Recycling of manganese gangue materials from waste-dumps in the Iberian Pyrite Belt-Application as filler for concrete production, Constr. Build. Mater. 54 (2014) 363–368.
[29] Z.H. Guo, Test and Constitution Relationship of Strength and Deformation of Concrete: Experimental Foundation and Constitutive Relations, Tsinghua University Press, Beijing, 1997.